

A magnetization and ^{11}B NMR study of $\text{Mg}_{1-x}\text{Al}_x\text{B}_2$ superconductors

M. Pissas¹, G. Papavassiliou¹, M. Karayanni¹, M. Fardis¹, I. Maurin², I. Margiolaki², K. Prassides^{1,2}, C. Christides^{1,3}

¹*Institute of Materials Science, NCSR, Demokritos, 153 10 Aghia Paraskevi, Athens, Greece*

²*School of Chemistry, Physics and Environmental Science, University of Sussex, Brighton BN1 9QJ, UK*

³*Department of Engineering Sciences, School of Engineering, University of Patras, 26110 Patras, Greece*

(Dated: October 31, 2018)

We demonstrate for the first time the magnetic field distribution of the pure vortex state in lightly doped $\text{Mg}_{1-x}\text{Al}_x\text{B}_2$ ($x \leq 0.025$) powder samples, by using ^{11}B NMR in magnetic fields of 23.5 and 47 kOe. The magnetic field distribution at $T = 5$ K is Al-doping dependent, revealing a considerable decrease of anisotropy in respect to pure MgB_2 . This result correlates nicely with magnetization measurements and is consistent with σ -band hole driven superconductivity for MgB_2 .

The synthesis of MgB_2 had been reported in 1954¹ but only recently Nagamatsu *et al.*² discovered that this compound is a superconductor with a surprisingly high $T_c \approx 39$ K. At first it was suggested³ that a BCS-type mechanism with strong electron-phonon coupling and high phonon energy of the light boron atoms can be responsible for the observed high- T_c . This is based on the observation of the isotope effect⁴ on T_c and a strong negative pressure coefficient of T_c .⁵ Alternatively, Hirsch⁶ proposed a "universal" mechanism where superconductivity in MgB_2 is driven by the pairing of dressed holes. Electronic band structure calculations^{3,7,8,9,10} indicate that in MgB_2 the charge carriers are situated in two bands derived from the σ -bonding $p_{x,y}$ -orbitals of boron, which are essentially two-dimensional (2D), and in one electron and one hole bands derived from the π -bonding p_z -orbitals of boron. Both, σ and π bands have strong in-plane dispersion due to the large overlap between all p orbitals of neighboring boron atoms. Despite some diversities in these models, there is a general agreement^{3,6,7,8,11,12} that the key point for superconductivity in MgB_2 is the 2D σ band of $p_{x,y}$ orbitals within the boron layers, and the delocalized metallic-type bonding between these layers. These calculations predict^{3,7,13,14,15} a strong anisotropy in the Fermi surface (and possibly in the electron phonon coupling) that is consistent with the observed^{15,16,17} anisotropy in H_{c2} . Specifically, the anisotropic ratio: $\gamma = H_{c2}^{ab}/H_{c2}^c$, was found^{15,17,18} to be between 1.7 and 6, depending on the material and the experimental method.

In view of this description, measurements on electron- or hole-doped MgB_2 are of interest as they may help our understanding of how the electronic density-of-states and the Fermi surface depend on doping. Al substitution for Mg in $\text{Mg}_{1-x}\text{Al}_x\text{B}_2$ provides a way for electron doping.^{19,20} The similarity of the calculated electronic density of states between MgB_2 and AlB_2 indicates that doping results in simple filling of the available electronic states, with one electron donated per Al.^{8,9,10} A very first study of Al doped MgB_2 showed¹⁹ that T_c is slightly suppressed for $x \leq 0.1$. However, band structure calculations show³ that there is a sharp drop in the density of states of MgB_2 at only slightly higher electron concentrations. Suzuki *et al.*^{9,10} predict that in $\text{Mg}_{1-x}\text{Al}_x\text{B}_2$ the concentration of σ holes varies with x as $n_h = (0.8 - 1.4x) \times 10^{22}$

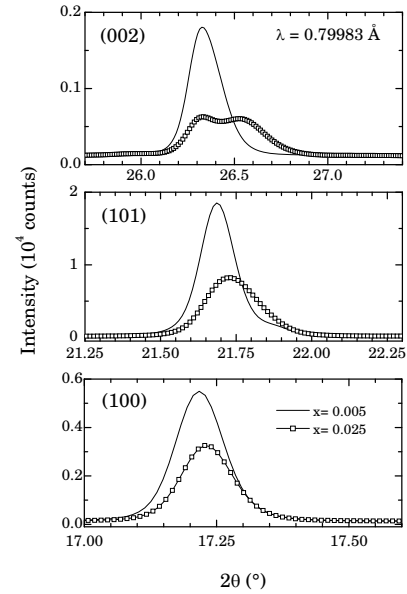


FIG. 1: Synchrotron X-ray diffraction ($\lambda = 0.79983$ Å) profiles showing the (002), (101) and (100) reflections for the $\text{Mg}_{1-x}\text{Al}_x\text{B}_2$ samples with $x = 0.005$ and 0.025 .

cm^{-3} , leading to $n_h = 0$ for $x \approx 0.6$. For $0.1 \leq x \leq 0.25$, a two phase mixture is formed, whereas for $x > 0.25$ a single non-superconducting phase is detected. The detrimental effect of doping on T_c in $\text{Mg}_{1-x}\text{Al}_x\text{B}_2$ can be explained within the BCS model, as it increases the Fermi energy (E_F) and decreases the density of states $N(E_F)$. Besides, thermoelectric power and resistivity measurements show²¹ that $\text{Mg}_{1-x}\text{Al}_x\text{B}_2$ alloys are hole-type normal metals. In order to analyze trends associated with the band filling and their relation to the loss of superconductivity, we have performed a detailed study of $\text{Mg}_{1-x}\text{Al}_x\text{B}_2$ ($0 \leq x \leq 0.1$) using structural, magnetic and ^{11}B NMR line shape measurements. Powder samples with nominal composition $\text{Mg}_{1-x}\text{Al}_x\text{B}_2$ ($0 \leq x \leq 1$) were prepared by liquid-vapor to solid reaction as described elsewhere.²² Synchrotron X-ray powder diffraction measurements were performed on $\text{Mg}_{1-x}\text{Al}_x\text{B}_2$ samples, sealed in thin-wall glass capillaries 0.5 mm in diame-

ter at 295 K.²³ Inspection of Figure 1 which shows parts of the XRD patterns of the $x = 0.005$ and 0.025 samples shows that while $\text{Mg}_{1.995}\text{Al}_{0.005}\text{B}_2$ is single phase, a clear splitting of the (002) reflection is observed for $\text{Mg}_{1.975}\text{Al}_{0.025}\text{B}_2$. This implies the onset of macroscopic phase separation with increasing Al content. A similar observation has been reported for C-doped MgB_2 compositions in which the carbon miscibility is also very small, $x < 0.04$.²⁴ For this reason we restrict our NMR study only to $\text{Mg}_{1-x}\text{Al}_x\text{B}_2$ samples with $x \leq 0.025$. The deduced lattice parameters are plotted in Fig. 2. For $x < 0.025$, the c -axis exhibits a negative slope $dc/dx \approx (-0.2 \text{ \AA/at \% Al})$, whereas the in-plane a -axis remains nearly constant. For $x \geq 0.025$, the coexisting phases differ mainly in their interlayer lattice constant.

Dc-magnetic measurements in a SQUID magnetometer under a magnetic field of $H = 10 \text{ Oe}$ show that all the examined samples are superconductors, with their T_c decreasing quasilinearly with increasing Al content ($dT_c/dx \approx -0.1 \text{ K/at \% Al}$). A steeper decrease of T_c is observed for $x > 0.1$ that becomes zero at $x \approx 0.55$. Figure 3 shows the reversible portion of the temperature dependence of the magnetization in various fields for $x = 0.01$. Contrary to high-temperature superconductors where fluctuation effects cause a substantial broadening of the transition with increasing temperature and field, the transition curves for $\text{Mg}_{0.99}\text{Al}_{0.01}\text{B}_2$ shift to lower temperatures in an almost parallel fashion. However, instead of the expected conventional linear dependence a pronounced curvature is present in $M(T)$ curves. This curvature has been attributed to the anisotropy^{17,18} of

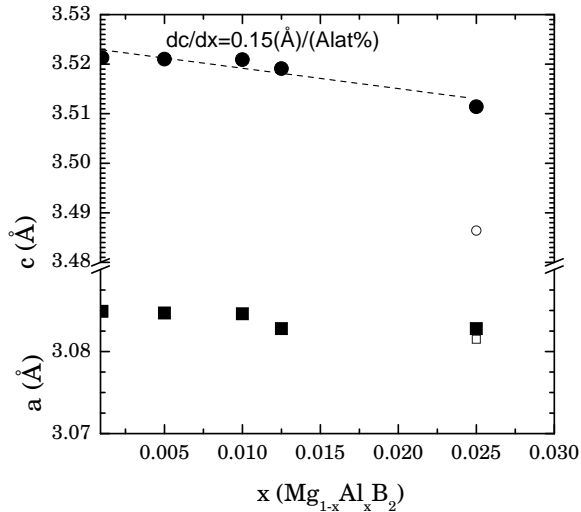


FIG. 2: Variation of the hexagonal unit cell parameters of $\text{Mg}_{1-x}\text{Al}_x\text{B}_2$ for $0 \leq x \leq 0.025$. Solid circles and squares correspond to the c - and a -axis of the $\text{Mg}_{1-x}\text{Al}_x\text{B}_2$ phase, respectively. The corresponding open symbols for $x = 0.025$ are the cell constants of the second $(\text{Mg}_{1-x}\text{Al}_x\text{B}_2)'$ phase (see main text)

MgB_2 . The dot-lines through the experimental points is a simulation of the reversible magnetic moment using the equation¹⁷:

$$4\pi M = -\frac{\Phi_0}{8\pi\lambda(T)^2\beta_A\gamma^{1/3}\sqrt{\gamma^2-1}} \times \left(\frac{1-4h^2}{3h^2}\sqrt{1-h^2} + \ln\left(\frac{1+\sqrt{1-h^2}}{h}\right) \right) \quad (1)$$

where $h = H/H_{c2}^{ab}$, $\lambda = (\lambda_{ab}^2\lambda_c)^{1/3}$ is the average penetration depth, $\beta_A = 1.16$, Φ_0 is the flux quantum, and $\gamma = H_{c2}^{ab}/H_{c2}^c$ is the anisotropy constant. In order to simulate the $M(T)$ data we suppose a power law relation for $H_{c2}^{ab}(T)$, $H_{c2}^{ab} = H_{c2}^{ab}(0)(1-T/T_c)^\nu$ (with $H_{c2}^{ab}(0) = 262 \pm 25 \text{ kOe}$, $T_c = 37.9 \pm 0.1 \text{ K}$ and $\nu = 1.27 \pm 0.05$), a weak magnetic field dependence, $\lambda \sim 2 \text{ nm}$, and an anisotropy constant $\gamma \sim 5.4$. Similarly, the $M(H)$ data have been simulated using the same γ and a temperature depended $\lambda(T)$. The value of the anisotropy constant, deduced from magnetic measurements, for $x = 0.01$ is *smaller than* that obtained from the $x = 0$ sample ($\gamma \sim 6$), in agreement with the NMR spectra (vide infra). The temperature variation of H_{c2}^{ab} has the same functional form with the $x = 0$ sample (i.e. the same exponent), while T_c and $H_{c2}^{ab}(0)$ are 0.7 K and 20 kOe smaller, respectively.

¹¹B NMR line shape measurements of the central transition ($-1/2 \rightarrow 1/2$) were performed on two spectrometers operating in external magnetic fields $H_o = 23.5$ and, 47 kOe . The spectra were obtained from the Fourier transform of half of the echo, following a typical $\pi/2 - \tau - \pi$ spin-echo pulse sequence. NMR is a very sensitive local probe of the spatially inhomogeneous magnetic field associated with the vortex state, which is formed in external magnetic fields $H_{c1} < H_o < H_{c2}$ ^{26,27}. In a recent study²⁵ we have observed that the ¹¹B NMR line shapes in pure MgB_2 remain unchanged down to the temperature of the second critical field T_{c2} whereas for $T < T_{c2}$, a second peak develops at lower frequencies. The intensity ratio of this second peak to the unshifted high-T peak was observed to increase in field $H_o = 23.5 \text{ kOe}$ when compared to that in field $H_o = 47 \text{ kOe}$ ²⁵. A direct comparison of the NMR line shapes with dc-magnetic measurements, that reveal the temperature dependence of H_{c2}^{ab} and H_{c2}^c , has shown that the intensity and shape of the low frequency peak follows the development of the vortex lattice as a function of temperature²⁵. Since in pure MgB_2 , $H_{c2}^{ab} \approx 150 \text{ kOe}$ ^{15,17}, this was explained as showing that a part of the grains remains in the normal state (unshifted peak) for $H_{c2}^c < H_o < H_{c2}^{ab}$ down to the lowest measured temperature $T = 5 \text{ K}$. It is thus remarkable that by light Al doping, the normal state signal component disappears in the mixed superconducting state and only the pure vortex lattice signal is present. This is clearly seen in Figure 4, which shows the ¹¹B NMR line shapes for $x = 0.01$ at various temperatures, in field 23.5 kOe . Alike to MgB_2 spectra²⁵, the line shapes in the normal state are temperature indepen-

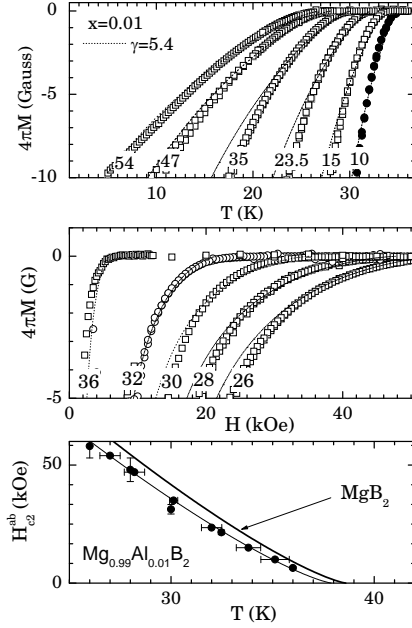


FIG. 3: (a) (upper panel) Zero field and field cooling magnetic moment as a function of the temperature for $10 \leq H \leq 54$ kOe for the powder $\text{Mg}_{0.99}\text{Al}_{0.01}\text{B}_2$ sample used in the NMR measurements. The dot-lines through the experimental points are simulations of the reversible magnetic moment supposing an anisotropy $\gamma \approx 5.4$ (see main text). (b) (middle panel) Isothermal magnetization loops in the reversible regime at $26 \leq T \leq 36$ K for $\text{Mg}_{0.99}\text{Al}_{0.01}\text{B}_2$. (c) (lower panel) Variation of H_{c2}^{ab} as a function of temperature for the $x = 0.01$ sample. The solid line is a fit through the experimental points with a power law relation $H_{c2}^{ab} = H_{c2}^{ab}(0)(1 - T/T_c)^\nu$ ($H_{c2}^{ab}(0) = 262 \pm 5$ kOe, $T_c = 37.9 \pm 0.1$ K and $\nu = 1.27 \pm 0.02$). Also included is the $H_{c2}^{ab}(T)$ -curve (thick solid line) of the $x = 0$ sample, for direct comparison.

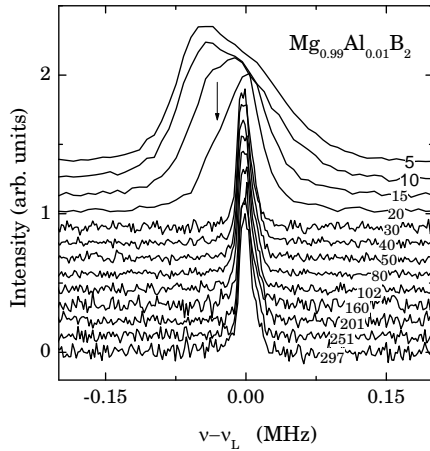


FIG. 4: ^{11}B NMR line shapes as a function of temperature for $\text{Mg}_{0.99}\text{Al}_{0.01}\text{B}_2$ under a magnetic field $H = 23.5$ kOe.

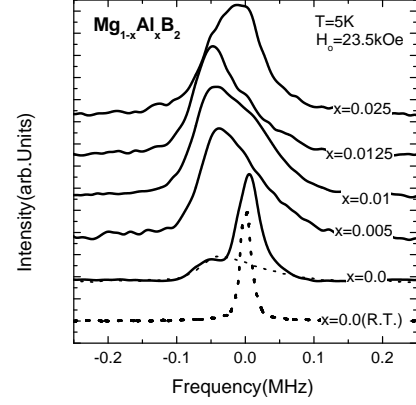


FIG. 5: ^{11}B NMR line shapes of $\text{Mg}_{1-x}\text{Al}_x\text{B}_2$ for $0.0 \leq x \leq 0.025$ at $T = 5$ K in field $H_0 = 23.5$ kOe.

dent. For $T \leq 30$ K the vortex lattice is formed, inducing a gradual shift of the peak frequency (corresponding to H_s) that creates the characteristic asymmetric broadening of the NMR frequency distribution as expected from the vortex lattice only.²⁷ This effect indicates an enhancement (relative to pure MgB_2) of H_{c2}^c above 23.5 kOe by Al doping, which leaves only the superconducting state at $T = 5$ K. At $T = 5$ K the shift of H_s from the field H_0 in the normal state is about 50 Gauss. Since we measure an anisotropic polycrystalline sample, it is expected that the sharp singularities smear out. It is worth noting that at $T = 20$ K the line shape exhibits a shoulder (see arrow in Fig. 4). This shoulder indicates that H_{c2}^c is crossed at this temperature.

Figure 5 shows NMR spectra at $T = 5$ K in $H_0 = 23.5$ kOe for $\text{Mg}_{1-x}\text{Al}_x\text{B}_2$ ($0 \leq x \leq 0.025$). At $T = 300$ K the NMR spectra are essentially identical for $0 \leq x \leq 0.2$. Since the cell constants change slightly in this concentration region, the observed similarity in the NMR spectra indicates that the induced line shape is resolution limited. At $T = 5$ K all the samples are in the mixed state and the line shape reflects the magnetic field distribution from the vortex lattice. Remarkably, the line shapes depend on x . As discussed above for the $x = 0$ system, the observed line shape is the result of the anisotropy. Hence, the disappearance of the normal state signal component and the variation of the vortex state signal with x can be explained by supposing that the anisotropy decreases with Al doping. We stress that even at $x = 0.005$ the component from the normal state signal disappears. In figure 5 we have scaled for comparison the signal intensity of the $x = 0.005$ system under the low frequency tail of pure MgB_2 . Apparently there is an excellent matching of the two signals, providing clear experimental evidence that this shoulder corresponds to the magnetic field distribution of the vortex state. We also notice that for $x \geq 0.025$ the line shape changes drastically. At this concentration either the anisotropy starts to increase abruptly, or the particular line shape is associated with the onset of

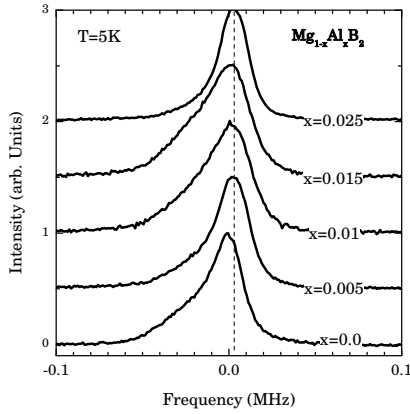


FIG. 6: ^{11}B NMR line shapes of $\text{Mg}_{1-x}\text{Al}_x\text{B}_2$ for $0.0 \leq x \leq 0.025$ at $T = 5\text{ K}$ in a magnetic field $H_o = 47\text{ kOe}$.

phase separation at this composition. Figure 6 shows the dependence of the NMR spectra on Al doping for $\text{Mg}_{1-x}\text{Al}_x\text{B}_2$ ($0 \leq x \leq 0.025$), at $T = 5\text{ K}$ and $H_o = 47\text{ kOe}$. Contrary to Figure 5, in all samples the line shapes exhibit a low frequency tail and an unshifted peak, corresponding to coexisting vortex and normal-state components. This indicates that $3.2 \leq \gamma \leq 6.4$ (e.g for $x = 0.01$ sample) by considering $H_{c2}^{ab} \approx 150\text{ kOe}$.

The observed decrease of anisotropy can be attributed to the progressive electron filling of the σ bands with in-

creasing x , which reduces the anisotropy of the boron p states. In the microscopic theory²⁸ the anisotropy parameter is given by $\gamma^2 = \langle \Delta(\mathbf{k}_F) v_{ab}^2 \rangle / \langle \Delta(\mathbf{k}_F) v_c^2 \rangle$, where v_i are the Fermi velocities and $\langle \dots \rangle$ stands for Fermi surface averages. When the ratio $\langle v_{ab}^2 \rangle / \langle v_c^2 \rangle$ is averaged over the entire Fermi surface for MgB_2 it is close to unity^{3,18}, which means a strong anisotropy of $\Delta(\mathbf{k}_F)$. Following the arguments of Bud'ko *et al.*¹⁸, the electron-phonon interaction is particularly strong on the Fermi surface sheets which are shaped as slightly distorted cylinders along the c crystal direction. If the gap Δ on the remaining Fermi surface sheets is negligible, the reduction of the anisotropy could originate from the reduction of the σ -holes, as we mentioned above.

In conclusion, we show for the first time the magnetic field distribution in the pure vortex state of lightly doped $\text{Mg}_{1-x}\text{Al}_x\text{B}_2$ by using ^{11}B NMR line shape measurements. Our NMR and magnetization data reveal that substitution of Al for Mg reduces the anisotropy substantially, apparently due to reduction of the σ -holes. This shows up the important role of $p_{x,y}$ orbitals (which form the $2D$ σ -holes band) in the superconductivity of MgB_2 . We argue that our results provide an experimental basis for further theoretical investigations concerning the role of the σ -bands in the superconducting mechanism of MgB_2 .

We thank the ESRF for provision of synchrotron X-ray beamtime and P. Pattison and I.A. Beukes for help with the experiments.

-
- ¹ M. Jones and R. March, J. Am. Chem. Soc. **76** 1434 (1954).
 - ² J. Nagamatsu *et al.*, Nature(London) **410**, 63 (2001); C. Buzea and T. Yamashita, cond-mat/0108265, (for a recent review).
 - ³ J. Kortus *et al.*, Phys. Rev. Lett. **86**, 4656 (2001).
 - ⁴ S. L. Bud'ko *et al.*, Phys. Rev. Lett. **86**, 1877 (2001); D. G. Hinks *et al.*, Nature **411**, 457 (2001).
 - ⁵ K. Prassides *et al.*, **64**, 012509 (2001); B. Lorenz, *et al.*, Phys. Rev. B **64**, 012507 (2001).
 - ⁶ J. E. Hirsch and F. Marsiglio, Phys. Rev. B **64**, 144523 (2001).
 - ⁷ J. M. An and W. E. Pickett, Phys. Rev. Lett. **86**, 4366 (2001).
 - ⁸ K. D. Belashchenko *et al.*, Phys. Rev. B **64**, 092503 (2001); K. D. Belashchenko Phys. Rev. B *et al.*, **64**, 132506 (2001).
 - ⁹ G. Satta *et al.*, Phys. Rev. B **64** 104507 (2001).
 - ¹⁰ S. Suzuki *et al.*, J. Phys. Soc. Jpn. **70**, 1206 (2001).
 - ¹¹ Y. Kong *et al.*, Phys. Rev. B **64** 020501(R) (2001).
 - ¹² P. P. Singh, Phys. Rev. Lett. **87**, 087004 (2001).
 - ¹³ Y. Wang *et al.*, Physica C **355**, 179 (2001).
 - ¹⁴ F. Bouquet *et al.*, Phys. Rev. Lett. **87**, 047001 (2001).
 - ¹⁵ O. F. de Lima *et al.*, Phys. Rev. Lett. **86**, 5974 (2001); S. Lee *et al.*, J. Phys. Soc. Jpn **70**, 2255 (2001); M. Xu *et al.*, Appl. Phys. Lett. **79**, 2779 (2001).
 - ¹⁶ S. Patnaik *et al.*, Supercond. Sci. Technol. **14**, 315 (2001).
 - ¹⁷ F. Simon *et al.*, Phys. Rev. Lett. **87**, 047002 (2001).
 - ¹⁸ S. L. Bud'ko *et al.*, Phys. Rev. B **64**, 180506 (2001).
 - ¹⁹ J. S. Slusky *et al.*, Nature (London) **410**, 343 (2001).
 - ²⁰ J. Y. Xiang *et al.*, cond-matt/0104366; J. Q. Li *et al.*, cond-matt/0104320; H. W. Zandbergen *et al.*, cond-matt/0109301;
 - ²¹ B. Lorenz *et al.*, Phys. Rev. B **64**, 052513 (2001).
 - ²² M. Pissas *et al.*, J. of Superconductivity **14**, 615 (2001) (cond-mat/0108153).
 - ²³ Images of the Debye-Scherrer rings were recorded on the 345 mm diameter Mar Research circular image plate system on the BM1A beamline at the ESRF, Grenoble. A monochromatic X-ray beam of wavelength, $\lambda = 0.79983\text{ \AA}$ and dimensions $0.5 \times 0.5\text{ mm}^2$ was focussed onto the sample by sagittal bending of the second crystal of the double-crystal Si (111) monochromator. Patterns were measured with sample-to detector distance of 200 mm for periods of 10 s. During the data collection the sample was rotated about its axis by 10° . One-dimensional diffraction patterns were obtained by integrating around the rings using local software (program FIT2D).
 - ²⁴ T. Takenobu *et al.*, Phys. Rev. B **64**, 134513 (2001); I. Maurin *et al.*, Physica B, in press.
 - ²⁵ G. Papavassiliou *et al.*, Phys. Rev. B (in press) (cond-mat/0107511).
 - ²⁶ W. Fite, and A. G. Redfield, Phys. Rev. Lett. **17**, 381 (1966).
 - ²⁷ E. H. Brandt and A. Seeger, Adv. Phys. **35**, 189 (1986).
 - ²⁸ L.P. Gor'kov and T.K. Melik-Barkhudarov, Zh. Eksp. Teor. Fiz. **45**, 1493 (1963)[Sov. Phys. JETP **18**, 1031 (1964)].